

A Greenland Sea perspective on the dynamics of post-convective eddies

K. I. C. Oliver^{1,5*}, T. Eldevik^{2,3}, D. P. Stevens⁴, and A. J. Watson¹

¹ School of Environmental Sciences, University of East Anglia, Norwich, U.K.

² Nansen Environmental and Remote Sensing Centre, Bergen, Norway.

³ Bjerknes Centre for Climate Research, Bergen, Norway.

⁴ School of Mathematics, University of East Anglia, Norwich, U.K.

⁵ Current affiliation: Department of Earth and Environmental Sciences, The Open University, Milton Keynes, U.K.

* Corresponding author. E-mail: k.i.c.oliver@open.ac.uk

Submitted to the *Journal of Physical Oceanography*

Abstract

Open ocean deep convection contributes to the formation of the dense waters that fill the global deep ocean. The dynamics of post-convective vortices are key to understanding the role of convection in ocean circulation. Submesoscale coherent vortices (SCVs) observed in convective regions are likely to be the anticyclonic components of hetons. Hetons are dipoles, consisting of a surface cyclone and a weakly stratified subsurface anticyclone, that can be formed by convection. Here, key post-convective processes are investigated using numerical experiments of increasing sophistication, with two primary goals: (1) to understand how the ambient hydrography and topography influence the propagation of hetons; (2) to provide a theoretical context for recent observations of SCVs in the Greenland Sea.

It is found that the alignment of hetons is controlled by ambient horizontal density gradients, and that hetons self-propagate into lighter waters as a result. This provides a mechanism for transporting convected water out of a cyclonic gyre, but the propagation is arrested if the heton meets large amplitude topography. Upon interaction with topography, hetons usually separate, and the surface cyclone returns towards denser water. The anticyclone usually remains close to topography and may become trapped for several hundred days. These findings may explain the observed accumulation and longevity of SCVs at the Greenland Fracture Zone, on the rim of the Greenland Sea gyre. The separation and sorting of cyclones from anticyclones have likely implications for the density and vorticity budgets of convective regions.

1 Introduction

Convection in the marginal seas of the North Atlantic Ocean has long been considered a key process in forming the dense waters which fill much of the global deep ocean. Overflow waters across the Greenland–Scotland ridge, feeding North Atlantic Deep Water, are formed through a combination of rapid heat loss in the Norwegian Sea, brine rejection through ice formation, and open ocean convection. It is now thought that only a modest component of overflow water is formed directly by deep convection in Greenland Sea (Mauritzen, 1996; Watson et al., 1999; Olsson et al., 2005). However, the densest water in the Nordic Seas is formed by Greenland Sea convection, and changes in deep convection have been linked to changes in the large scale dense water properties of the region on multi-decadal timescales (Bönisch et al., 1997). These waters are too dense to overflow the Greenland–Scotland ridge until they mix with lighter waters aloft, and therefore provide a lower boundary condition on intermediate waters of overflow density. Therefore, the influence of the Greenland Sea on the larger scale circulation is likely to be on multi-decadal timescales.

Understanding convective regions depends on the understanding of post-convective dynamics. It is unusual to observe ongoing deep convection, and the majority of evidence for convection is obtained from observing post-convective vortices (Kasajima et al., 2006), or regional–scale stratification (Ronski and Budeus, 2005), weeks or months after convection has ceased. Moreover, the post-convective behaviour of vortices is likely to be a key control on the heat and salinity budgets of convective regions (Legg et al., 1996). Post-convective dynamics have been the focus of previous process studies (e.g. Legg and Marshall, 1998; Gryanik et al., 2000), but these have been in the context of a uniform ambient hydrography. In

practice, convection occurs in cyclonic gyres with significant horizontal density gradients, and bounded by steep topography, each of which have the potential to influence the behaviour of post-convective vortices.

The topography and mean circulation of the Greenland Sea is plotted in Figure 1. The Greenland Sea is flanked by land or shallow (<2500 m) topography on all sides. Warm saline Atlantic water is carried northward to the east of the Greenland Sea in the West Spitsbergen Current, recirculates in Fram Strait and the Arctic Ocean, and flows southward as part of the East Greenland Current (EGC). The EGC also carries cold fresh waters of polar origin. This large scale cyclonic circulation around the Nordic Seas is ultimately wind-driven with a strong barotropic component (Furevik and Nilsen, 2005), but there is also significant vertical shear in the flow; for example, the transport along the Arctic front to the south-east is dominated by its baroclinic component (Oliver and Heywood, 2003). The Greenland Sea itself consists of the Greenland Basin and the Boreas Basin, separated by the Greenland Fracture Zone (GFZ). The Greenland Sea gyre refers to the cyclonic circulation in the Greenland Basin, and this has usually been the focus of studies of Greenland Sea convection, but deep convection has also been observed to occur in the Boreas Basin (Johannessen et al., 2005). There is topographically steered cyclonic circulation in each basin (Jakobsen et al., 2003), and waters of polar and Atlantic origin are observed over the GFZ as a result (Quadfasel and Meincke, 1987). This wind-driven circulation leads to the doming of isopycnals towards the gyre centre, generating horizontal density gradients. Weak stratification at the gyre centre and baroclinic instability in the rim current have long been viewed as the properties of cyclonic gyres that favour deep convection (Killworth, 1979).

Rapidly rotating lenses of weakly stratified water have been observed in the Greenland Sea (Gascard et al., 2002; Wadhams et al., 2004; Budéus et al., 2004; Kasajima et al., 2006; Ronski and Budeus, 2006), as well as in the Labrador Sea (Gascard, 1983; Pickart et al., 1996; Lilly et al., 2003) and Mediterranean Sea (Testor and Gascard, 2006). These anticyclones have the defining characteristics of submesoscale coherent vortices (SCVs; McWilliams, 1985): they are smaller than mesoscale eddies, have been observed to survive for over a year (Wadhams et al., 2004), and have a velocity maximum at mid-depths. In convective regions, they are likely to be the anticyclonic components of hetons (see Figure 2). Hetons are baroclinic dipoles which, experiments in laboratory tanks and numerical models suggest, are produced by deep convection (Marshall and Schott, 1999), or by topographic interactions (Dewar, 2002a). (For clarity, in this study we only use the expression “SCV” when discussing observations, and otherwise refer to hetons and their cyclonic and anticyclonic components.) Several Greenland Sea SCVs have been observed on the western flank of the GFZ, and at least two long-lived and near-stationary SCVs have been observed near $75^{\circ}\text{N } 0^{\circ}\text{E}$, west of the southern tip of the GFZ (Gascard et al., 2002; Wadhams et al., 2004; see Figure 1). This may be interpreted as evidence that convection is localised there, but an alternative hypothesis is that the local topography and hydrography causes post-convective vortices to accumulate and/or survive for longer near the GFZ.

The goals of this study are to improve the understanding of how ambient hydrography and topography influence post-convective vortices, and to assess the impact of the dynamics of these vortices on the interpretation of observations from the Greenland Sea. In Section 2, we briefly summarise existing dynamical theory of vortices in convective regions, and the relevance of this theory to the Greenland

Sea. In Section 3, the experiments are presented. Channel experiments are used to develop an understanding of the interaction of hetons both with ambient flow and topography. More realistic basin experiments are used to assess implications of these results for the Greenland Sea, particularly with regard to the observed distribution of SCVs. Our key findings are summarised in Section 4.

2 Background to the dynamics of post-convective vortices

2.1 Heton formation and propagation

Open ocean deep convection occurs through highly localised plumes of upwelling and downwelling water. The integrated properties of a convective patch can be characterised in terms of an unstably stratified volume undergoing rapid vertical mixing (Send and Marshall, 1995). Numerical experiments suggest that such a mixed patch exchanges buoyancy with its stratified surroundings, both during and after convection, through baroclinic instability and the shedding of hetons (Legg et al., 1996). Figure 2 is a schematic representing the processes that lead to the formation and propagation of a heton. At the instant of formation, a heton is a vertically aligned dipole, consisting of a cyclone directly overlying an anticyclone. This may be understood in terms of the redistribution of potential vorticity (Legg and Marshall, 1993), or in terms of geostrophic shear: the weakly stratified heton is a buoyant anomaly at depth, causing anticyclonic shear, and a dense anomaly at the surface, causing cyclonic shear.

Of interest here is the propagation and coherence of hetons that are not subject to ongoing convection, either because surface buoyancy loss has ceased, or they have left the convective patch. Hetons self-propagate if they are not vertically aligned. For example, the surface cyclone in Figure 2c lies to the left of the sub-surface anticyclone, causing self-propagation into the page. The name “heton”

derives from the heat transport associated with this self-propagation (Hogg and Stommel, 1985), and the theory describing the behaviour of hetons in a rotating uniformly stratified fluid is well developed (e.g. Griffiths and Hopfinger, 1986; Legg and Marshall, 1993; Carton, 2001). Gryanik et al. (2000) developed a quasi-geostrophic theory for isolated hetons, with equal magnitude cyclonic and anti-cyclonic components, in uniform stratification and zero ambient shear. The heton propagates with velocity:

$$c_h = C(b, h) U_h, \quad (1)$$

where $C(b, h)$ is a function of the horizontal vortex separation b (non-dimensionalised by the bulk Rossby radius, L_R), and the convection depth h (non-dimensionalised by the bathymetric depth H). The velocity scale U_h is determined by the strength of the initial mixed patch:

$$U_h = \frac{L_R}{T_h} = \frac{f^2 A \overline{g'}}{4\pi H^2 N^3}, \quad L_R = \frac{NH}{f}, \quad T_h = \frac{4\pi H^3 N^4}{f^3 A \overline{g'}}, \quad (2)$$

where f is the Coriolis parameter, N is the ambient buoyancy frequency, T_h is a timescale, A is the horizontal area of the initial vertically aligned heton, and $\overline{g'}$ is the mean buoyancy anomaly in the initial mixed patch, so that $A\overline{g'}$ is the total buoyancy anomaly per unit depth (Gryanik et al. (2000) actually derived U_h in terms of a vorticity source rather than a buoyancy anomaly). For large horizontal separations between the cyclone and the anticyclone ($b \gg 1$), $C \sim b^{-1}$; for full details see Gryanik et al. (2000).

2.2 Vortex interaction with ambient flow and topography

The baroclinic rim current around convective patches plays a key role in generating and propagating hetons (Legg and Marshall, 1993). Theory and numerical experiments suggest that the density transport across narrow fronts scales with the

time-mean along-front geostrophic velocity and the horizontal density gradient (e.g. Visbeck et al., 1996; Spall and Chapman, 1998). On the other hand, Legg and Marshall (1998) found that a larger scale barotropic cyclonic gyre circulation, such as is generally found in convection regions, stabilises the frontal region in a heton model. This reduced the efficiency of cross-frontal density transport by heton generation. This experiment has not been repeated for a baroclinic gyre. Walsh and Pratt (1995) derived a point-vortex model in which asymmetric but like-signed point vortices could propagate relative to the ambient flow in the presence of vertical shear; this propagation was in a direction parallel to the ambient flow. However, Kasajima et al. (2006) speculated that vertical shear in the ambient flow contributes to the observed rapid migration of SCVs *across* the ambient flow in the Greenland Sea, citing tropical cyclones as a similar atmospheric process. Tropical cyclones consist of a surface cyclone and an upper atmosphere anticyclone. There is evidence that there is propagation to the left (in the Northern Hemisphere) of the ambient vertical velocity shear (Wu and Emanuel, 1993): the upper anticyclone is displaced downstream of the lower cyclone, forming a baroclinic dipole which then self-propagates in the direction of flow between the vortices. In Section 3, we test the hypothesis that an analogous process acts on hetons.

There have been many studies of the interaction of vortices with topography in the context of the opposite limiting cases of barotropic and surface-trapped vortices. A barotropic mesoscale vortex over a topographic slope is subject to topographic β -drift (Carnevale et al., 1991; Flór and Eames, 2002), comparable to westward vortex drift on a β -plane. Over strong slopes, vortices can become stationary and surface-trapped due to dispersion at depth in topographic waves

(LaCasce, 1998). Surface-trapped vortices that exceed the Rossby radius may be stabilised by steep topography. Hetons are neither barotropic nor surface-trapped, with a velocity maximum at mid-depths in the anticyclone. Jacob et al. (2002) found that analytical theories that successfully predict the propagation of barotropic or monopolar baroclinic vortices break down in the case of counter-rotating vortices such as hetons, and argued that an experimental approach was needed to understand their behaviour. The role of isolated topography in the generation and evolution of hetons was examined by Dewar (2002a). Hetons could survive over weak topography, with sizable propagation rates influenced by topography. In the setting of full-column convection in a quasi-geostrophic model, Dewar (2002b) found that heton formation is inhibited by weak slopes, but that steep slopes can repulse anticyclones due to advection of ambient potential vorticity across isobaths by the heton. Following partial-column convection, however, slope effects were more disorganised, but even weak slopes were able to slow dispersal of hetons.

3 Numerical experiments

Numerical experiments were designed with the objectives of understanding the effects of ambient horizontal density gradients and bathymetry on the behaviour of post-convective vortices, both in a general context and in the Greenland Sea specifically. For this reason, mixed-patch release experiments were carried out in a simple channel setting, as well as in basin experiments more closely representing the Greenland Sea. All experiments were carried out with the Massachusetts Institute of Technology general circulation model (MITgcm; Marshall et al., 1997) on an f -plane ($f = 1.5 \times 10^{-4} \text{ s}^{-1}$). The vertical resolution of the 40 levels decreased from 11 m at the surface to 147 m at the bottom (3750 m), and a very high hori-

zonal resolution of 500×500 m was applied in order to resolve post-convective vortices. The parameterised biharmonic horizontal viscosity was $3 \times 10^6 \text{ m}^4 \text{ s}^{-1}$ and the Laplacian horizontal tracer diffusivity was $0.2 \text{ m}^2 \text{ s}^{-1}$, in each case as low as stability constraints would permit. The vertical viscosity and diffusivity was $1 \times 10^{-5} \text{ m}^2 \text{ s}^{-1}$. The model was allowed to spin-down from a prescribed initial state in geostrophic equilibrium. In the experiments presented here, the energy loss to the system was typically $\sim 10\%$ in 200 days, so the effect of this spin-down is unlikely to qualitatively affect the results. The exclusion of wind and surface buoyancy forcing simplifies interpretation of results at the expense of neglecting processes that are likely to influence the behaviour of vortices. Because no buoyancy forcing was applied, and the equation of state was linear, we refer directly to density as the active tracer.

3.1 Mixed patch release

We first describe the release of a mixed patch, common to both channel and basin experiments. Columns of homogeneous water with a radius of 6 grid-cells (3 km) were added to an ambient density field by increasing the density above 1300 m to equal the density at 1300 m. (The initialisation of the ambient field is described for channel and basin experiments in Sections 3.2 and 3.3 respectively.) The depth of 1300 m approximates the bottom of the well mixed layer of Greenland Sea Intermediate Water, overlying slightly more stratified water (Naveira Garabato et al., 2004; Ronski and Budeus, 2005), observed in the Greenland Sea. The mixed-patches represent the integral product of buoyancy–forced convection (Send and Marshall, 1995), and were tagged with a tracer. The initial velocity field was not altered to be in geostrophic equilibrium with the mixed patch, implying an assumed timescale for convection of less than f^{-1} . While this assumption may not

be realistic, the products of mixed-patch releases closely resemble the results of laboratory and numerical model convection experiments.

Figure 3 shows the initial behaviour of a released mixed patch from a Greenland Sea basin experiment with idealised-bathymetry (Section 3.3.3), but is representative also of other experiments. Snapshots of the velocity, tracer, and density fields at Day 0 (mixed-patch release), Day 10 and Day 20 are presented. The mixed-patch is initially a density anomaly with no velocity signature, but it sinks and forms a heton (comparable to the schematic in Figure 2). Most of the tracer marking the mixed patch is contained within the weakly stratified deep anticyclone, which is associated with a buoyant anomaly below the centre of mass of the tracer. A surface cyclone also forms, associated with the upper ocean dense anomaly. This is consistent with the schematic provided in Figure 2, and with laboratory and numerical experiments (Narimousa, 1998; Marshall and Schott, 1999). The cyclone mostly contains water from outside the initial mixed patch. The anticyclone and cyclone separate, and after 20 days do not horizontally overlap. The relative velocities of the anticyclone and cyclone are consistent with separation caused by vertical shear in the ambient flow. Due to ambient horizontal density gradients, the surface cyclone is advected downstream more rapidly than the sub-surface anticyclone. The absolute velocity of the heton, however, cannot be explained entirely in terms of advection by the ambient flow. There is a component to the right of the ambient velocity field, which is consistent with heton self-propagation. If the alignment of the heton is set by the ambient density gradients, then the density gradients ultimately control the self-propagation of the heton. Hetons would then be expected to self-propagate towards lighter water. This line of evidence is developed in Section 3.2.2.

3.2 Periodic channel experiments

3.2.1 Experiment design

Idealised experiments were first carried out in a 80×200 km channel, periodic in the longer dimension. A zonal section of bathymetry and initial hydrography for the standard “flat bottom” experiments is plotted in Figure 4. Vertical steps of 1000 m exist 10 km from each zonal boundary in order to provide some topographic stabilisation of the flow in the presence of density gradients (Spall, 2004); with an entirely flat bottom, eddies rapidly remove the zonal structure in the hydrography. Additionally, Figure 4 shows bathymetry in “sloping bottom” experiments, where bottom depth H is described by

$$\frac{f}{H} \frac{\partial H}{\partial x} = -\beta_H, \quad 3750 \text{ m} > H > 1700 \text{ m}, \quad (3)$$

where $H(40 \text{ km}) = 2700 \text{ m}$, and β_H is the topographic beta associated with barotropic processes, and H is uniform in y . $\beta_H = 1.7 \times 10^{-9} \text{ (m s)}^{-1}$ in the standard sloping bottom experiment.

Density decreases from west to east at the surface, and exponentially decays, with an e-folding scale of 700 m, towards a uniform value at infinite depth. Therefore denser water overlies deeper topography, mimicking convective basins such as the Greenland Sea. Smoothed random perturbations were added to the density field, an example of which can be seen in contours in Figure 5a, but otherwise the hydrography was meridionally uniform. Over a bathymetric depth of 2700 m, the top-to-bottom density difference was 0.095 kg m^{-3} . This initial field is consistent with observations of the Greenland Sea (Oliver and Heywood, 2003), except for the observed narrow stratified summer surface layer. The initial surface velocity had baroclinic and barotropic components of equal magnitude and direction, which were in geostrophic equilibrium (except for any released mixed patches, as

described in Section 3.1), so that flow was northward along isobaths.

In additional experiments, used to investigate the role of vertical shear strength, initial horizontal density gradients were scaled according to

$$\rho(x, y, z) = \rho_{std}(40 \text{ km}, y, z) + S_\rho \left(\rho_{std}(x, y, z) - \rho_{std}(40 \text{ km}, y, z) \right), \quad (4)$$

where S_ρ is the scaling factor and ρ_{std} was obtained from the standard experiment. Additionally, “uniform N^2 ” experiments (which produces unrealistic hydrography including strong density gradients at the bottom) were set-up specifically to facilitate comparison with the Gryanik et al. (2000) theory. In these experiments

$$\rho(x, y, z) = \rho_{var}(x, y, z_e) + (z - z_e) \overline{(\rho_z)_{var}}, \quad (5)$$

where $z_e = -500$ m, ρ_{var} was obtained from the standard experiment (with variable N^2), and $\overline{(\rho_z)_{var}}$ is the mean vertical density gradient between depths 300 m and 1400 m at $x = 40$ km in the standard experiment’s initial field. The 300 m and 1400 m levels were chosen because these depths approximate the centre of cyclones and anticyclones, respectively.

3.2.2 Vortex propagation

Figure 5 shows snapshots of the density field in the standard flat-bottom experiment with two mixed patches released. Both mixed patches form hetons which are advected to the north by the ambient flow, but also propagate to the east towards lighter water, until approaching steep topography at $x = 70$ km. Both the cyclone and the anticyclone are visible as distinct features although they propagate together. The cyclones are located to the north and west of the anticyclones, causing heton self-propagation to the east and north. This supports the hypothesised role of ambient hydrography in heton propagation, discussed in Section 2.2.

This experiment was repeated under identical conditions, except that the geostrophic shear scaling $S_\rho = 1$ was replaced by $S_\rho = \frac{1}{2}$, 2 and 4 respectively. Trajectories of the heton-pairs from each experiment are plotted in Figure 6a. The rate of northward propagation is approximately proportional to the horizontal stratification, simply because the ambient flow is stronger where there is greater geostrophic shear. It is less straightforward to explain why the rate of eastward propagation, prior to meeting topography or heton separation, is also greater in the experiments with stronger shear. The ability of the Gryanik et al. (2000) theory to explain these results is tested using the theoretical eastward propagation rate:

$$c_g = C(b, h) U_h \cos \theta, \quad (6)$$

where θ is the angle between due north and the vector from the anticyclone to the cyclone. 10-day mean eastward propagation rates were compared with propagation rates c_g predicted by (6). These are plotted as circles in Figure 6b for the experiment plotted in 6a, as well as for repeats with different random perturbations in the initial field. Where the heton has met topography, or anticyclones and cyclones have separated, results are not plotted. U_h and h vary little with S_ρ , so the predicted eastward propagation rate can only be decreased either by increasing the distance between the cyclone and anticyclone (we typically find $b > 1$), or by rotating the cyclone so it is no longer aligned north of the anticyclone. Rotation is an important source of variability, especially in the $S_\rho = \frac{1}{2}$ experiment where westward propagation may even occur due to the cyclone moving south of the anticyclone. This may suggest that the surface cyclone is stronger than the sub-surface anticyclone, which would cause cyclonic rotation of a heton (Carton, 2001).

Model propagation rates are well correlated ($R^2 > 0.6$ for each experiment)

with predicted rates from Gryanik et al. (2000), but are systematically slower; however, comparison is inhibited by the variability of stratification in the model. Uniform N^2 experiments, described in Section 3.2.1, are used to test the theory more rigorously. (Note, however, that even in these experiments a uniform N^2 is not preserved as the density field evolves. After 30 days, N^2 outside hetons has a standard deviation of $\sim 20\%$.) Again, a good correlation between model and theory is obtained (although $R^2 = 0.48$ for $S_\rho = 4$) but propagation rates in the model are slower. Least-squares fitting, with a forced zero-intercept, shows that the theory overestimates propagation rate more strongly in experiments with weak horizontal density gradients (Figure 6b). Thus, while the model qualitatively agrees with the Gryanik et al. (2000) theory, the theory is unable to fully explain the relationship between density gradients and propagation rates.

3.2.3 The influence of topography

The behaviour of hetons becomes more complex in the presence of topography. In the “flat bottom” experiments, the anticyclonic and cyclonic components of the hetons separate upon reaching steep topography at $x = 70$ km. The cyclones then propagate towards denser water, in some cases eventually reaching a position west of the release point at $x = 30$ km (not shown). The anticyclones typically remain close to the topography at $x = 70$ km until they lose coherence. The mechanism for the separation of cyclones and anticyclones is explored further in Section 3.3.5.

Figure 6c is a repeat of Figure 6a, but for experiments with a standard sloping bottom (Figure 4; $\beta_H = 1.7 \times 10^{-9} \text{ (m s)}^{-1}$). The initial behaviour is qualitatively similar to the flat bottom experiments, but the topography provides a potential vorticity barrier, slowing and eventually arresting eastward propagation. A further

effect of sloping topography is the stabilisation of the ambient flow (c.f. Spall, 2004). As a result of the reduced eddy kinetic energy (EKE), the longevity of vortices is typically increased in the presence of sloping topography. Trajectories of a heton in the absence of ambient density gradients, but with a sloping bottom, are also plotted in Figure 6c. No clear pattern of propagation is found in this case, or two repeats (not shown) with different initial random perturbations. (Analogous experiments were also run in the flat bottom configuration, but the heton could remain static and vertically aligned for at least 300 days.)

Several studies (e.g. Dewar, 2002b; LaCasce, 1998) have obtained qualitatively different vortex behaviour, depending on the steepness of the slope. Here, we consider four different slope steepness parameters (in addition to the vertical steps in the “flat bottom” experiments). The range $0.425 \times 10^{-9} \leq \beta_H \leq 3.4 \times 10^{-9}$ encompasses the range applied by Dewar (2002b). In Figure 6d, the propagation of the anticyclones is plotted for the 4 different bottom slopes. While the behavior is qualitatively similar in each experiment, the rate of propagation decreases monotonically with slope steepness. In each experiment, eastward propagation is retarded and eventually arrested at a point approximately 10 km west of the 2000 m isobath. In the $\beta_H = 0.425 \times 10^{-9}$ experiment, the anticyclone then quickly loses coherence, associated with the relatively high ambient EKE due to the weak slope. In the $\beta_H = 3.4 \times 10^{-9}$ experiment, the anticyclone appears to briefly become trapped shortly after its eastward propagation ceases. Repeat experiments (not shown) show that this does not invariably occur with this domain. This behaviour is discussed further in Section 3.3.4. One difference between our experiments and the experiments of Dewar (2002b) is that Dewar made this comparison under full depth convection, whereas our experiments represent partial

water column convection. This may explain why we find no qualitative difference in propagation over shallow and steep slopes.

3.3 Basin experiments

3.3.1 Experiment design

The results of the channel experiments are placed in the context of the Greenland Sea using basin experiments. Two alternative domains were used. In an “idealised bathymetry” experiment, the key topographic features of the Greenland Sea (the Greenland Basin, the Boreas basin, the GFZ and the Greenland continental slope) were represented in a simplified form. In a “realistic bathymetry” experiment, 1 km resolution GEBCO bathymetry (IOC et al., 2003) was used. A sloping wall was added at the edge of the domain, except where the Greenland continental slope provides a natural boundary, to provide a closed basin. In both experiments, the 500×500 m resolution was applied in the central 200×200 km only, decreasing to 1500×1500 m resolution at the edge of the domain (see Figures 7 and 10 for the idealised and realistic bathymetry experiments, respectively). The domains were rotated so that Greenland was to the north, rather than the north-west (this does not affect results on an f -plane).

Initial densities and barotropic velocities followed bathymetry, using the same approach applied in the “sloping bottom” channel experiment (Section 3.2.1). However, in the basin experiments the hydrography and velocity fields were smoothed to damp the effect of small-scale topography on the density and velocity fields, and no random perturbation was added. The alignment of density contours and streamlines with topography yielded a cyclonic circulation in the initial field. Unlike the channel experiments, however, the 200 day output from the control experiment was used for mixed-patch release rather than the initial field. This is because

it was found that significant reorganisation of the flow occurred within the first 100 days. The mixed-patch population was added in the form of a grid, making the location of each member of the population somewhat arbitrary. In reality, the onset of convection is likely to depend both on the initial stratification and on the local vorticity field. However, the location of convection in the Greenland Sea is not well established, and the application of an arbitrary grid of mixed patches avoids biasing the conclusions of this study.

3.3.2 Ambient hydrographic and velocity fields

In the channel experiments, the key controls of hydrography and topography on heton propagation were established for a highly idealised setting. In this section, we explore the importance of these mechanisms for convective regions such as the Greenland Sea. We begin with a control experiment (without mixed patches), with an idealised representation of the bathymetry in the Greenland Sea. This is preferable to advancing immediately to accurate bathymetry, because the detail of a realistic field may inhibit understanding of the key controls of topography on the simulations. Instead, we represent only those features which we hypothesise to be of major importance to the behaviour of post-convective vortices: the Greenland and Boreas basins, the GFZ and the Greenland continental slope.

Figure 7a shows bathymetric contours, as well as mean density and velocity fields, in the idealised bathymetry simulation. Figure 7b shows the corresponding eddy kinetic energy (EKE) field. Density contours and streamlines approximately follow isobaths, including around the GFZ. (This result does not depend on light water overlying the GFZ in the initial field; if dense water is initially placed over the GFZ, it is replaced by lighter water on a timescale of less than

100 days.) This is consistent with observational evidence from floats (Jakobsen et al., 2003), and from the anomalously warm water found on the northeastern flank of the GFZ (Quadfasel and Meincke, 1987), indicating a source from the East Greenland Current (EGC). The dominant larger scale circulation feature is cyclonic flow encompassing both the Boreas Basin and the Greenland Basin. Additionally there are closed cyclonic streamlines within each basin. There can be no EGC distinct from the Greenland Sea gyre, because of the closed boundaries used. Possibly associated with this, the Greenland Sea gyre centre is displaced towards Greenland and away from the GFZ, if compared with observations (Figure 1). The location of the fronts is sensitive to the exact choice of initial field, and varies temporally in the real Greenland Sea also (Budéus et al., 1993). The model also produces a mean broad anticyclone near the centre of the Greenland Basin, which is a strong feature. Although float data (Poulain et al., 1996) and current observations (Oliver and Heywood, 2003) suggest that the local flow often opposes the larger scale mean circulation, it is doubtful that such a strong mean feature exists in the real Greenland Sea. Figure 7b shows that EKE is greatest where there are strong density gradients and weak topographic gradients. Despite strong density gradients at the GFZ, steep topography there stabilises the flow.

3.3.3 Vortex propagation and the role of the Greenland Fracture Zone

We now present results in which the control simulation is seeded with a grid of 25 mixed patches. Figure 8 is a spaghetti diagram of the trajectories of the anti-cyclonic component of hetons formed from these mixed patches, both before and after heton separation (note that Day 0 is the time of release of the mixed patches, equivalent to Day 200 in the control experiment). The majority of vortices ini-

tially propagate in a cyclonic direction around the gyre, but with a component away from the gyre centre. However, some vortices are initially within, or close to, anticyclonic features, such as the large anticyclone in the centre of the Greenland Sea. These propagate in an anticyclonic direction and towards the centre of the anticyclonic feature. These results are consistent with advection by the ambient flow and propagation towards lighter water, as obtained in the channel experiments.

The process of propagating towards lighter water is further illustrated in Figure 9. This shows time series of the density at 400 m above each of 25 anticyclones. The initial rapid decrease in density is caused primarily by sinking of the mixed patch and separation of the cyclone after release, and partly by initial self-propagation. Therefore, each time-series is referenced to the density at Day 20 in order to emphasise later evolution that is affected only by propagation into waters of different density. Decreasing density at 400 m above the anticyclones indicates that anticyclones propagate into lighter ambient water. The channel experiments predict that the rate of propagation into lighter water is affected by the magnitude of the ambient density gradient, and by the presence of topography. This is consistent with Figure 9, which shows that the rate at which anticyclones move into lighter water is highly variable, and in some cases very small due to weak ambient gradients. The change in ambient density is also small when vortices encounter topography; the highlighted examples of anticyclones A and C, marked in Figures 8 and 9, show that the density above these anticyclones changes little after they reach the GFZ. Nevertheless, of the 25 anticyclones released, the only four which move into denser water do so while in the process of losing coherence. All vortices which retain coherence move into lighter water.

From these results, we conclude that the anticyclonic component of a convectively–formed heton in a cyclonic gyre will propagate out of that gyre unless it is trapped within a larger scale anticyclone feature or by topography. In the Greenland Sea, the Greenland continental slope and the GFZ are the two main topographic barriers, and vortices that reach the Greenland continental slope are likely to be swept out of the gyre in the EGC. Figure 8 suggests that the GFZ catches the anticyclonic component of hetons that would otherwise depart the gyre. The tendency for anticyclones to accumulate near the GFZ is exacerbated by the longevity of anticyclones that reach the GFZ. Anticyclones in regions of high EKE (Figure 7b) are more likely to lose coherence than those in low EKE regions such as the GFZ. Upon reaching the GFZ, some vortices are advected around the GFZ by the ambient flow (anticyclones B, D and E in Figure 8). However, anticyclone A remains almost stationary for 140 days until it interacts with B and both vortices lose coherence. Anticyclone C remains almost stationary from Day 20 until the end of the simulation (Day 300), merging with anticyclone D around Day 120. Both of these stationary anticyclones are found within anticyclonic meanders in the ambient flow, which are mean features in the control experiment (Figure 7).

3.3.4 Realistic bathymetry experiments

Figure 10a shows the mean density field in the realistic bathymetry control experiment. Most features are in agreement with the idealised bathymetry experiment, although the anticyclone at the centre of the Greenland Sea is a much weaker feature. Another notable difference is that density is not as clearly defined by bathymetry at the GFZ, allowing the mean flow to cross the GFZ before reaching its southern tip. This is probably because the GFZ is not a continuous topographic

feature at its maximum amplitude, which is how it is represented in the idealised bathymetry. However, it does not follow that the importance of the GFZ is exaggerated in the idealised bathymetry experiment and correctly diagnosed in the realistic bathymetry experiment. The flow around and over the GFZ is dependent on the relative importance of barotropic and baroclinic flow, which is not well constrained by observations. The limited existing evidence, summarised in Figure 1, suggests that the GFZ is a greater obstacle to the mean flow than obtained in the realistic bathymetry experiment. As with the idealised basin experiment, the centre of the cyclonic gyre is further from the GFZ than observations suggest, which increases the length of closed streamlines around the gyre.

Figure 10b shows anticyclone trajectories in the mixed-patch release experiment. Again, most of the features of the idealised bathymetry experiment are repeated here, with propagation into lighter water and a tendency for anticyclones to exit the gyre. Accumulation at the GFZ also occurs. Anticyclone F merges with G, and anticyclone H merges with I, and these vortices become trapped on the western flank of the GFZ. The region where these vortices accumulate is slightly to the north of where the mean flow begins to cross the GFZ in the simulation, and ~ 80 km north of the location where, in reality, the greatest number of SCVs have been observed. This is the site of a pre-existing larger scale anticyclonic meander, a feature common to trapped anticyclones in the idealised-bathymetry experiment and channel experiment. Once inside such a meander, an anticyclone cannot migrate downstream of the meander without either climbing bathymetry or propagating into denser water, whereas we have found that anticyclones propagate into lighter water but that this propagation is halted by steep slopes. We also note that trapping is found only where there is steep topography ($\beta_H > 3 \times 10^{-9}$ (m

s)⁻¹) immediately upslope of the vortex, in both channel and basin experiments. Insofar as such scenarios are comparable with vortex–wall interactions, this would be expected to promote propagation to the right of the upslope direction (Dewar, 2002b), against the ambient flow.

3.3.5 Sorting of cyclones and anticyclones

The separation of cyclones and anticyclones upon interaction with topography, followed by the return of cyclones to denser water, is a remarkably consistent feature in both channel and basin experiments. This occurs whether the heton approaches a large vertical step, a steep slope, or a gradual slope. Identified exceptions, where the heton remains unseparated despite retardation of heton propagation by topography, are rare and limited to cases where density gradients are weak and therefore heton propagation is slow, such as the $S_\rho = \frac{1}{2}$ case in Figure 5c. (Note, however, that heton separation may also occur without apparent interaction with topography, such as in the $S_\rho = 4$ case in Figure 5a.) The initial stage of this process, heton separation, is consistent with the skewing of the vorticity field due to the control of topographic beta on potential vorticity. Dewar (2002b) argued that this process suppressed heton formation over a slope in quasi-geostrophic experiments with uniform ambient density. Dewar, however, did not obtain downslope propagation of cyclones.

In order to understand the behaviour of the lone vortices after separation, we consider the propagation of asymmetric monopolar vortices. Walsh (1995), using a quasi-geostrophic model in the context of “Meddies”, found that tilting of vortices due to the ambient velocity shear can cause self-propagation of vortices, provided that there is also a vertical gradient in the vorticity of the vortex. This

is because the tilting creates a mean horizontal asymmetry, with the stronger (for example) vorticity aloft unaligned with the weaker vorticity below. The residual vorticity field, after the dominant symmetric component is removed, is similar to a baroclinic dipole. A barotropic residual dipole may also exist due to horizontal asymmetries in the vortex. Such a vortex is termed a quasi-monopole (Stern and Radko, 1998), and is sketched in Figure 11a.

Here, we examine the residual vorticity field of 38 anticyclones and 26 cyclones, taken from all available experiments, in a vertical plane parallel with isobaths. Vortices were chosen that could clearly be identified to have recently separated (defined as a distance of >25 km between the centres of the anticyclones and cyclones) from their anticyclonic partner, following interaction with topography. Figure 11b and 11c show composite residual vorticity fields for the cyclones and anticyclones respectively. The composites were obtained by rotating in the vertical axis of each vortex so that upslope is into the page. The mean asymmetry in the composite anticyclone, with positive vorticity to the left of the vortex centre, would indicate upslope propagation, but spatial variability dominates this signal. However, the mean cyclone exhibits a coherent asymmetric component consistent with downslope propagation. (Individual cyclones do not always exhibit such asymmetry, and there were approximately 4 cases of asymmetry of the opposite sign). The asymmetry is principally barotropic, rather than baroclinic, suggesting that topographic rather than vertical shear effects are responsible. In laboratory tank experiments Voropayev et al. (1999) found that a quasi-monopole will propagate away from a wall following a collision, due to rearrangement of vorticity within the vortex. It is surprising, however, that the clearest asymmetry in our experiments is to be found in the surface cyclone, rather than the subsurface

anticyclone which is more directly influenced by topography.

4 Concluding remarks

This study provides evidence that the ambient hydrography and topography are key controls on the propagation of post-convective vortices, and the associated transport of convected waters. Ambient density gradients determine the direction of self-propagation of hetons, by controlling the relative positions of their cyclonic and anticyclonic components. Thus, in our simulations, hetons move towards lighter water and typically out of gyres that are host to convection, providing a mechanism for removing convected water from convective regions. This propagation is arrested at steep topography, where subsurface anticyclones accumulate. A subset of anticyclones that reach such topography become trapped within anticyclonic meanders in the mean flow; these remain stationary and coherent for several hundred days. The cyclonic components of hetons do not accumulate at topography, but return to denser waters after heton separation.

Several simplifying assumptions have been made in this study. Most importantly, the roles of wind and ongoing surface buoyancy forcing have been excluded. The significant non-linearity of the equation of state in the Greenland Sea has also been neglected. Furthermore, the experiment setup minimizes the impact of convection on the ambient density field. Large scale convective patches would be expected to generate strong baroclinic rim currents which are likely to contribute to the propagation of hetons away from sites of convection (Legg and Marshall, 1993). Nevertheless, the experiments are sufficiently sophisticated that existing analytical theories cannot be used to quantitatively predict the results. The behaviour of hetons under scenarios differing greatly from the presented experiments is therefore uncertain. For example, the propagation of hetons formed after

full-depth convection has not been investigated. On the other hand, when mixed patches with horizontal scales exceeding the local Rossby radius were released (not shown), the mechanisms discussed here applied after the mixed patches divided into multiple hetons. A small number of experiments, not presented here, were conducted in the setting of stronger vertical stratification. The Gryanik et al. (2000) theory predicts that self-propagation speed has a weak dependence on ambient vertical density stratification (varying as N^{-1} if convection depth is constant). Instead, we found that self-propagation into lighter waters was almost negligible in high stratification experiments.

With these caveats in mind, we consider the likely implications of our findings on the interpretation of observations in convective regions. Testor and Gascard (2006) observed the spreading phase of deep-convection by following floats inside post-convective vortices. Floats in the North Balearic Front were advected rapidly by the ambient flow, but there was a component of propagation towards warmer waters (their Figure 15), whereas floats nearer steep topography propagated more slowly or not at all. These results are consistent with the mechanisms described in this study, although the preponderance of anticyclones observed by Testor and Gascard (2006) suggests that many of the propagating anticyclones may not have been part of heton-pairs. In the Greenland Sea, SCVs have been observed in the highest concentrations at the rim of the gyre, and particularly at the GFZ (Gascard et al., 2002; Wadhams et al., 2004; Kasajima et al., 2006). Our results indicate that this is not strong evidence that the SCVs were initially produced by convection close to the GFZ, because anticyclones formed closer to the gyre centre may also accumulate at the GFZ. High concentrations of weakly stratified SCVs at the GFZ may rather precondition the region for deep convection:

convection has been observed within a pre-existing SCV at the GFZ (Wadhams et al., 2004). Observations also show that at least two SCVs have become trapped close to $75^{\circ}\text{N } 0^{\circ}\text{E}$ (Gascard et al., 2002), leading to speculation that the local topography favours the trapping of SCVs. In our simulations, some anticyclones were trapped within larger scale anticyclonic meanders near the GFZ. The trapped SCV observed by Gascard et al. (2002) appears to be located within a larger scale anticyclonic feature (indicated by minima in the depth of isopycnals immediately outside the SCV in Figure 3 of Gascard et al.). Other SCV surveys have not covered a large enough area to test this hypothesis. In the idealised bathymetry basin experiment, one anticyclone became trapped in a position analagous to $75^{\circ}\text{N } 0^{\circ}\text{E}$ immediately downstream of the tip of the GFZ, but this was not reproduced in the realistic bathymetry basin experiment. A more robust result is that the site of an already trapped anticyclone can interact with further anticyclones that are advected around the GFZ. In our experiments, there is one example of vortex dissipation and three examples of merging as a result of such interactions, suggesting that the site of a trapped SCV is a favourable location for the trapping of further SCVs.

Acknowledgements

This study was supported by a UK NERC Rapid programme grant (NER/T/S/2002/00446) and by Norwegian Research Council project ProClim (155923/700). We thank Igor Esau, Jonathan Lilly and Fiamma Straneo for discussion on the manuscript. This is publication no. A193 from the Bjerknes Centre for Climate Research.

References

- Bönisch, G., J. Blindheim, J. L. Bullister, P. Schlosse, and D. W. R. Wallace, 1997: Long-term trends of temperature, salinity, density, and transient tracers in the central Greenland Sea. *J. Geophys. Res.*, **102 (C8)**, 18 553–18 571.
- Budéus, G., B. Cisewski, S. Ronski, D. Dietrich, and M. Weitere, 2004: Structure and effects of a long lived vortex in the Greenland Sea. *Geophys. Res. Lett.*, **31**, L05 304, doi:10.1029/2003GL017 983.
- Budéus, G., A. A. Maul, and G. Krause, 1993: Variability in the Greenland Sea as revealed by a repeated high-spatial-resolution conductivity-temperature-depth survey. *J. Geophys. Res.*, **98 (C6)**, 9,985–10,000.
- Carnevale, G. F., R. C. Kloosterziel, and G. J. F. van Heijst, 1991: Propagation of barotropic vortices over topography in a rotating tank. *J. Fluid Mech.*, **233**, 119–139.
- Carton, X., 2001: Hydrodynamical modeling of oceanic vortices. *Surv. Geophys.*, **22**, 179–263.
- Dewar, W. K., 2002a: Baroclinic eddy interaction with isolated topography. *J. Phys. Oceanogr.*, **32**, 2789–2805.
- Dewar, W. K., 2002b: Convection in small basins. *J. Phys. Oceanogr.*, **32**, 2766–2788.
- Drange, H., T. M. Dokken, T. Furevik, T. R. Gerdes, and W. Berger, (Eds.) , 2005: *The Nordic Seas: An integrated perspective*. Geophysical Monograph Series **158**, AGU.

- Eldevik, T., F. Straneo, A. B. Sandø, and T. Furevik, 2005: Pathways and export of Greenland Sea water. Drange et al. (2005), 89–104.
- Fahrbach, E., J. Meincke, S. Østerhus, G. Rohardt, U. Schauer, V. Tcerberg, and J. Verduin, 2001: Direct measurements of heat and mass transport through Fram Strait. *Polar Research*, **20**, 217–224.
- Flór, J. B. and I. Eames, 2002: Dynamics of monopolar vortices on a topographic beta-plane. *J. Fluid Mech.*, **456**, 353–376.
- Furevik, T. and J. E. O. Nilsen, 2005: Large-scale atmospheric circulation variability and its impacts on the Nordic Seas ocean climate - a review. Drange et al. (2005), 105–136.
- Gascard, J. C., A. J. Watson, M. J. Messias, K. A. Olsson, T. Johannessen, and K. Simonsen, 2002: Long-lived vortices as a mode of deep ventilation in the Greenland Sea. *Nature*, **416**, 525–527.
- Gascard, R. A., J. C. Clarke, 1983: The formation of Labrador Sea Water. Part II: Mesoscale and smaller-scale processes. *J. Phys. Oceanogr.*, **13**, 1779–1797.
- Griffiths, R. W. and E. J. Hopfinger, 1986: Experiments with baroclinic vortex pairs in a rotating fluid. *J. Fluid Mech.*, **173**, 501–518.
- Gryanik, V. M., T. N. Doronina, D. J. Olbers, and T. H. Warncke, 2000: The theory of three-dimensional hetons and vortex-dominated spreading in localized turbulent convection in a fast rotating stratified fluid. *J. Fluid Mech.*, **423**, 71–125.
- Hogg, N. G. and H. M. Stommel, 1985: The heton, an elementary interaction

between discrete baroclinic geostrophic vortices, and its implications concerning eddy heat-flow. *Proc. R. Soc. Lond.*, **397**, 1–20.

IOC, IHO, and BODC, 2003: Centenary edition of the GEBCO digital atlas. Published on CD-ROM on behalf of the Intergovernmental Oceanographic Commission and the International Hydrographic Organization as part of the General Bathymetric Chart of the Oceans; British Oceanographic Data Centre, Liverpool.

Jacob, J. P., E. P. Chassignet, and W. K. Dewar, 2002: Influence of topography on the propagation of isolated eddies. *J. Phys. Oceanogr.*, **32**, 2848–2868.

Jakobsen, P. K., M. Ribergaard, D. Quadfasel, T. Schmith, and C. Hughes, 2003: Near-surface circulation in the northern North Atlantic as inferred from Lagrangian drifters: Variability from the mesoscale to interannual. *J. Geophys. Res.*, **108** (C8), doi:10.1029/2002JC001554.

Johannessen, O. M., K. Lygre, and T. Eldevik, 2005: Convective chimneys and plumes in the northern Greenland Sea. Drange et al. (2005), 251–272.

Kasajima, Y., K. A. Olsson, Johannessen, T., M.-J. Messias, E. Jeansson, R. G. J. Bellerby, and I. Skjelvan, 2006: A submesoscale coherent eddy in the Greenland Sea in 2003. *J. Geophys. Res.*, **111**, doi:10.1029/2005JC003130.

Killworth, P. D., 1979: On “chimney” formation in the ocean. *J. Phys. Oceanogr.*, **9**, 531–554.

LaCasce, J. H., 1998: A geostrophic vortex over a slope. *J. Phys. Oceanogr.*, **28**, 2362–2381.

- Legg, S., H. Jones, and M. Visbeck, 1996: A heton perspective of baroclinic eddy transfer in localized open ocean convection. *J. Phys. Oceanogr.*, **26**, 2251–2266.
- Legg, S. and J. Marshall, 1993: A heton model of the spreading phase of open-ocean deep convection. *J. Phys. Oceanogr.*, **23**, 1040–1056.
- Legg, S. and J. Marshall, 1998: The influence of the ambient flow on the spreading of convected water masses. *J. Mar. Sci.*, **56**, 107–139.
- Lilly, J. M., P. B. Rhines, F. S. Schott, K. Lavendar, J. Lazier, U. Send, and E. D’Asaro, 2003: Observations of the Labrador Sea eddy field. *Prog. Oceanogr.*, **59**, 75–176.
- Marshall, J., C. Hill, L. Perelman, and A. Adcroft, 1997: Hydrostatic, quasi-hydrostatic, and nonhydrostatic ocean modeling. *J. Geophys. Res.*, **102 (C3)**, 5733–5752.
- Marshall, J. and F. Schott, 1999: Open-ocean convection: Observations, theory, and models. *Rev. Geophys.*, **37**, 1–64.
- Mauritzen, C., 1996: Production of dense overflow waters feeding the North Atlantic across the Greenland-Scotland Ridge. Part 2: An inverse model. *Deep-Sea Res. I*, **43**, 807–836.
- McWilliams, J. C., 1985: Submesoscale, coherent vortices in the ocean. *Rev. Geophys.*, **23**, 165–182.
- Messias, M.-J., et al., 2008: The Greenland Sea Tracer Experiment 1996-2002: horizontal mixing and transport of Greenland Sea Intermediate Water. *Prog. Oceanogr.*, doi:10.1016/j.pocean.2007.06.005.

- Narimousa, S., 1998: Turbulent convection into a linearly stratified fluid: the generation of subsurface anticyclones. *J. Fluid Mech.*, **354**, 101–121.
- Naveira Garabato, A. C., K. I. C. Oliver, A. J. Watson, and M. J. Messias, 2004: Turbulent diapycnal mixing in the Nordic seas. *J. Geophys. Res.*, **109** (C12), C12 010.
- Nøst, O. A. and P. E. Isachsen, 2003: The large-scale time-mean ocean circulation in the Nordic Seas and Arctic Ocean estimated from simplified dynamics. *J. Mar. Res.*, **61**, 175–210.
- Oliver, K. I. C. and K. J. Heywood, 2003: Heat and freshwater fluxes through the Nordic Seas. *J. Phys. Oceanogr.*, **33**, 1009–1026.
- Olsson, K. A., E. Jeansson, T. Tanhua, and J. C. Gascard, 2005: The East Greenland Current studies with CFCs and released sulphur hexafluoride. *J. Mar. Syst.*, **55**, 77–95.
- Pickart, R. S., W. M. Smethie, J. R. Lazier, E. P. Jones, and W. J. Jenkins, 1996: Eddies of newly formed upper Labrador Sea water. *J. Geophys. Res.*, **399**, 20 711–20 726.
- Poulain, P.-M., A. Warn-Varnas, and P. P. Niiler, 1996: Near-surface circulation of the Nordic seas as measured by Lagrangian drifters. *J. Geophys. Res.*, **101** (C8), 18 237–18 258.
- Quadfasel, D. and J. Meincke, 1987: Note on the thermal structure of the Greenland Sea gyres. *Deep-Sea Res. A*, **34**, 1883–1888.
- Ronski, S. and G. Budeus, 2005: Time series of winter convection in the Greenland Sea. *J. Geophys. Res.*, **110**, doi:10.1029/2004JC002 318.

- Ronski, S. and G. Budeus, 2006: Vertical structure reveals eddy lifetime in the Greenland Sea. *J. Geophys. Res.*, **33**, doi:10.1029/2006GL026045.
- Send, U. and J. Marshall, 1995: Integral effects of deep convection. *J. Phys. Oceanogr.*, **25**, 855872.
- Spall, M. A., 2004: Boundary currents and watermass transformation in marginal seas. *J. Phys. Oceanogr.*, **34**, 1197–1213.
- Spall, M. A. and D. C. Chapman, 1998: On the efficiency of baroclinic eddy heat transport across narrow fronts. *J. Phys. Oceanogr.*, **28**, 2275–2287.
- Stern, M. E. and T. Radko, 1998: The self-propagating quasi-monopolar vortex. *J. Phys. Oceanogr.*, **28**, 22–39.
- Testor, P. and J.-C. Gascard, 2006: Post-convection spreading phase in the Northwestern Mediterranean Sea. *Deep-Sea Res.*, **53**, 869–893.
- Visbeck, M., J. Marshall, and H. Jones, 1996: Dynamics of isolated convective regions in the ocean. *J. Phys. Oceanogr.*, **26**, 1721–1734.
- Voropayev, S. I., G. B. McEachern, D. L. Boyer, and H. J. S. Fernando, 1999: Experiment on the self-propagating quasi-monopolar vortex. *J. Phys. Oceanogr.*, **29**, 2741–2751.
- Wadhams, P., G. Budéus, J. P. Wilkinson, T. Løyning, and V. Pavlov, 2004: The multi-year development of long-lived convective chimneys in the Greenland Sea. *Geophys. Res. Lett.*, **31**, L06306, doi:10.1029/2003GL019017.
- Walsh, D., 1995: A model of a mesoscale lens in large-scale shear. Part I: Linear calculations. *J. Phys. Oceanogr.*, **25**, 735–746.

- Walsh, D. and L. J. Pratt, 1995: The interaction of a pair of point potential vortices in uniform shear. *Dyn. Atm. Oceans*, **22**, 135–160.
- Watson, A. J., et al., 1999: Mixing and convection in the Greenland Sea from a tracer-release experiment. *Nature*, **401**, 902–904.
- Woodgate, R. A., E. Fahrbach, and G. Rohardt, 1999: Structure and transports of the East Greenland Current at 75°N from moored current meters. *J. Geophys. Res.*, **104 (C8)**, 18 059–18 072.
- Wu, C. C. and K. A. Emanuel, 1993: Interaction of a baroclinic vortex with background shear: application to hurricane movement. *J. Atmos. Sci.*, **50**, 62–76.

Figure Captions List

Figure 1: Topography and schematic of the mean intermediate depth circulation of the Greenland Sea and its environs. Marked isobaths are 1000, 2500, 3000, and 3500 m. Abbreviations for marked features are GB - Greenland Basin; BB - Boreas Basin; GFZ - Greenland Fracture Zone; EGC - East Greenland Current; WSC - West Spitsbergen Current; X - location where long-lived stationary SCVs have been observed (Gascard et al., 2002; Wadhams et al., 2004). Dashed arrows indicate currents that are either less well established by observations or less permanent. Studies on which the schematic is based include results from a tracer release experiment (Messias et al., 2008), observations from floats (Poulain et al., 1996; Gascard et al., 2002; Jakobsen et al., 2003), moored and lowered current meters (Woodgate et al., 1999; Fahrbach et al., 2001; Oliver and Heywood, 2003), hydrographic observations (Quadfasel and Meincke, 1987), and modelled reconstructions of the circulation of the Nordic Seas (Nøst and Isachsen, 2003; Eldevik et al., 2005).

Figure 2: Vertical section–view schematic of the formation of a heton. Shading represent layers of water defined by density. (a) Surface buoyancy forcing causes local densification of the surface layer, represented here as a column of well mixed water reaching from the surface to the base of the intermediate water layer. (b) The well mixed patch sinks. Geostrophic shear results in anticyclonic rotation within the mixed patch and cyclonic rotation aloft. (c) The cyclone and anti-cyclone separate, forming a baroclinic dipole, or a “heton”. SCVs in convective regions are anticyclones thought to be formed in this way. The heton propagates in the direction of flow between the cyclone and the anticyclone (into the page, in this example). Arrows indicate a possible control on the alignment of hetons: we argue in Section 3 that the alignment, and therefore the propagation, of hetons is controlled by the vertical velocity shear resulting from ambient density gradients.

Figure 3: Time series of the response to the release (Day 0) of a mixed patch. Left panels show a plan view of tracer (marking the initial mixed patch) evolution, with velocity vectors at a spacing is 4 grid points (2 km). Central panels show vertical sections of tracer distribution, with density contours (black dashed contour spacing is 0.01 kg/m^3 ; separation between the two solid black contours is 0.05 kg/m^3). Right panels show cross-section velocity sections (positive flow into the page). The relative position of the plan-view and section plots is indicated by white lines. Vertical section alignment is chosen to pass through both the anticyclone and the cyclone. Note that the domain centres move horizontally with the anticyclone centre.

Figure 4: Section of initial density in the standard experiment. Density is relative to maximum (bottom) value. Bathymetry for “flat bottom” experiment is shown; the bold line is the bathymetry for standard sloping bottom experiment.

Figure 5: Density time slices from the early part of a mixed patch release experiment in the standard flat-bottom channel set-up. Density is at 1500 m, relative to the maximum density in the experiment. At this depth the anticyclones are lighter than the ambient water, and cyclones are denser than the ambient water. This level is below the maximum depth of the mixed patches before release (at $x = 30$ km, $y = 100$ km, and $x = 55$ km, $y = 10$ km). Black contours are for density at 400 m, and depict the upper ocean positive density anomaly associated with both cyclones and anticyclones.

Figure 6: Trajectories of anticyclones and cyclones in (a) flat bottom experiments, and (c) sloping bottom experiments ($\beta_H = 1.7 \times 10^{-9}$). Trajectories are plotted for experiments where the horizontal stratification is scaled by $S_\rho = \frac{1}{2}, 1, 2$ and 4 respectively, relative to the standard experiment. Numbers indicate the day at which the vortex reached the specified location. An “X” indicates that the vortex has lost coherence. (b) - Model versus theoretical eastward propagation rates in flat bottom experiments. Colours indicate different values of S_ρ , matching those in (a) and (c). Circles are for variable N^2 experiments and stars for uniform N^2 experiments (see text). (d) - Trajectories of anticyclones in experiments over different values of slope steepness parameter β_H , with $S_\rho = 1$.

Figure 7: 200-400 day fields of (a) mean density, with velocity vectors (b) eddy kinetic energy ($\text{cm}^2 \text{s}^{-2}$; log scale) in the idealised bathymetry basin control experiment at 1250 m depth. Density is relative to the densest water in the basin. Velocity vectors are plotted at one twentieth of the resolution of the grid in both dimensions. 2000 m and 3000 m isobaths are plotted in white in (a); 2500 m and 3000 m isobaths are plotted in black in (b). The representation of the Greenland Basin (GB), the Boreas Basin (BB) and the GFZ are labelled in (b); the direction of north has been rotated so that the Greenland continental slope is at the upper limit of the plot.

Figure 8: Spaghetti plot of anticyclone trajectories in the idealised bathymetry basin mixed-patch release experiment. Shading indicate number of days since the release of mixed patches. Some anticyclones lose coherence before the end of the experiment. 2500 m and 3000 m isobaths are plotted in black. Anticyclones that accumulate at the GFZ are labelled next to the start of their trajectories. Notable larger scale features are also labelled, where the horizontal density gradient is reversed relative to the general increase in density towards the geographical gyre centre (see Figure 7).

Figure 9: Evolution of density above each anticyclone at 400 m, referenced to density at Day 20 (after initial adjustment is complete), in the idealised bathymetry basin experiment. Incomplete tracks indicate that the anticyclone lost coherence. Anticyclones A and C (see Figure 8) are plotted with bold dashed lines.

Figure 10: (a) 200-400 day mean density field in the realistic bathymetry basin control experiment at 1250 m depth. Density is relative to the densest water in the basin. 2500 m and 3000 m isobaths are plotted in black. (b) Spaghetti plot of anticyclone trajectories in the realistic bathymetry mixed-patch release basin experiment. Shading indicates the number of days since the release of mixed patches. Some anticyclones lose coherence before the end of the experiment. Anticyclones that become trapped at the GFZ are labelled in bold type next to the start of their trajectories.

Figure 11: (a) - Plan view schematic of a quasi-monopole (after Voropayev et al., 1999). The arrow shows the direction of self-propagation. (b) - Vertical section of asymmetric relative vorticity, ζ , component (residual after symmetric component removed) through a composite of 26 surface cyclones that have recently separated from subsurface anticyclones upon interaction with topography. Section is viewed looking upslope. Dark shading indicates $\zeta > 0.3 \times 10^{-5}$; light shading indicates $0.3 \times 10^{-5} > \zeta > -0.3 \times 10^{-5}$. White shading indicates $\zeta < -0.3 \times 10^{-5}$. Implied dipole propagation, due to vortex asymmetry, is downslope (towards the reader). (c) - As (b) but a composite of 38 anticyclones.

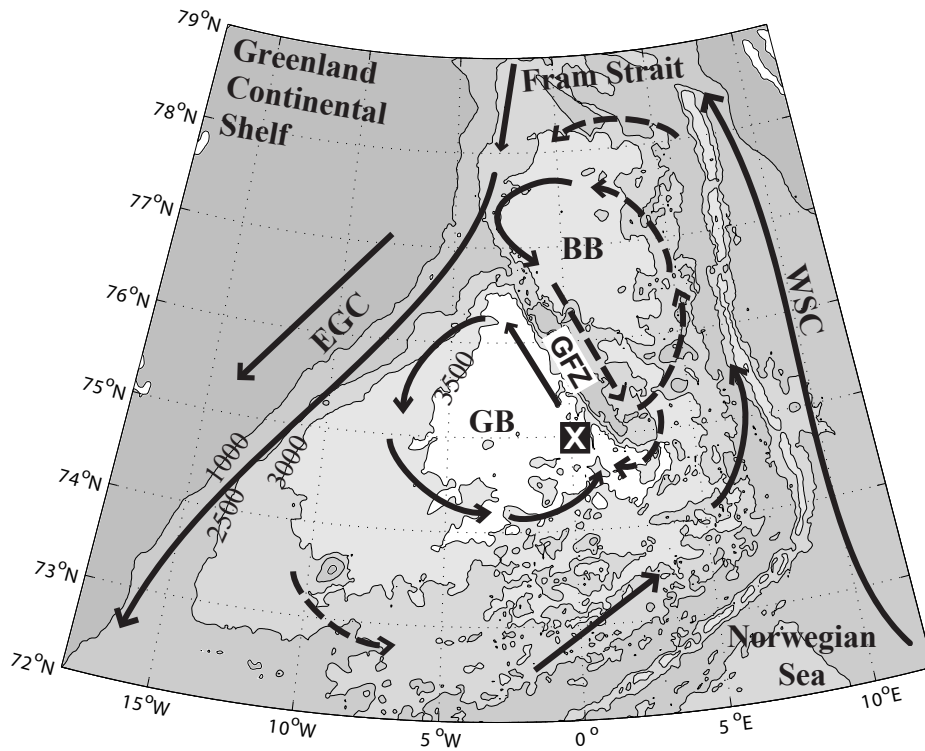


Figure 1: Topography and schematic of the mean intermediate depth circulation of the Greenland Sea and its environs. Marked isobaths are 1000, 2500, 3000, and 3500 m. Abbreviations for marked features are GB - Greenland Basin; BB - Boreas Basin; GFZ - Greenland Fracture Zone; EGC - East Greenland Current; WSC - West Spitsbergen Current; X - location where long-lived stationary SCVs have been observed (Gascard et al., 2002; Wadhams et al., 2004). Dashed arrows indicate currents that are either less well established by observations or less permanent. Studies on which the schematic is based include results from a tracer release experiment (Messias et al., 2008), observations from floats (Poulain et al., 1996; Gascard et al., 2002; Jakobsen et al., 2003), moored and lowered current meters (Woodgate et al., 1999; Fahrbach et al., 2001; Oliver and Heywood, 2003), hydrographic observations (Quadfasel and Meincke, 1987), and modelled reconstructions of the circulation of the Nordic Seas (Nøst and Isachsen, 2003; Eldevik et al., 2005).

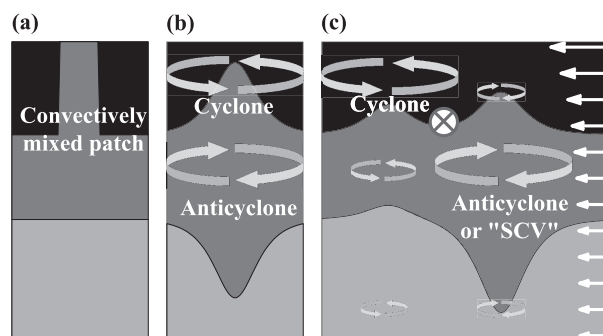


Figure 2: Vertical section–view schematic of the formation of a heton. Shading represent layers of water defined by density. (a) Surface buoyancy forcing causes local densification of the surface layer, represented here as a column of well mixed water reaching from the surface to the base of the intermediate water layer. (b) The well mixed patch sinks. Geostrophic shear results in anticyclonic rotation within the mixed patch and cyclonic rotation aloft. (c) The cyclone and anticyclone separate, forming a baroclinic dipole, or a “heton”. SCVs in convective regions are anticyclones thought to be formed in this way. The heton propagates in the direction of flow between the cyclone and the anticyclone (into the page, in this example). Arrows indicate a possible control on the alignment of hetons: we argue in Section 3 that the alignment, and therefore the propagation, of hetons is controlled by the vertical velocity shear resulting from ambient density gradients.

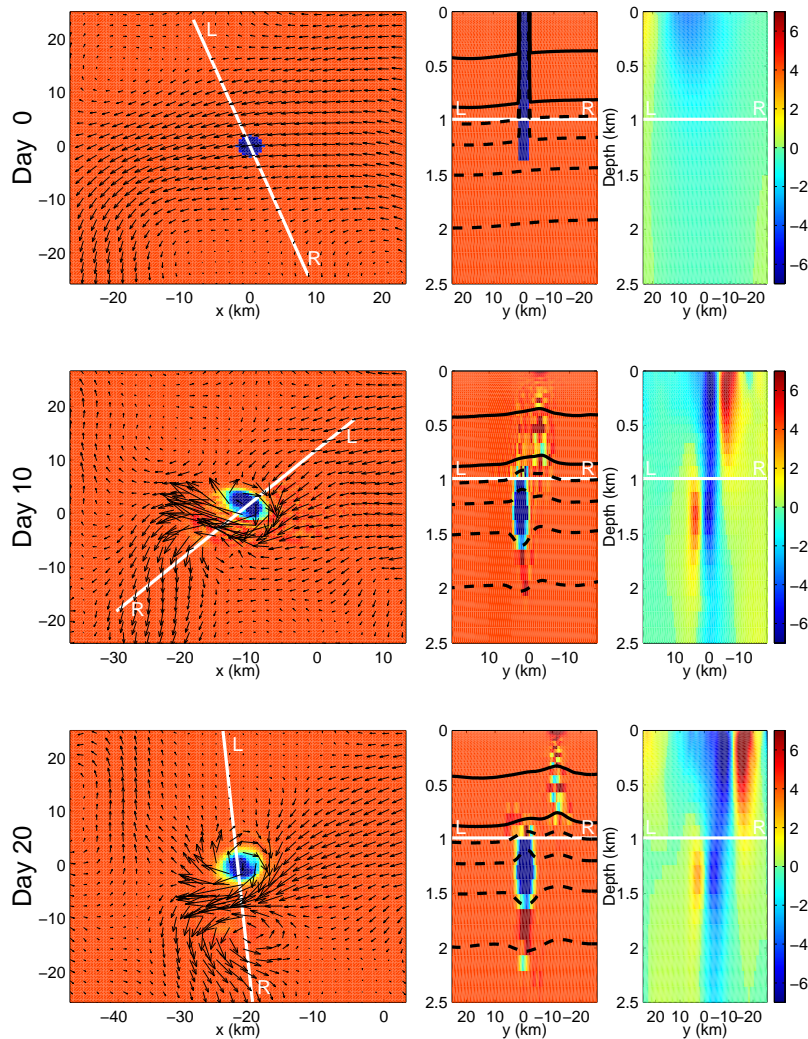


Figure 3: Time series of the response to the release (Day 0) of a mixed patch. Left panels show a plan view of tracer (marking the initial mixed patch) evolution, with velocity vectors at a spacing is 4 grid points (2 km). Central panels show vertical sections of tracer distribution, with density contours (black dashed contour spacing is 0.01 kg/m^3 ; separation between the two solid black contours is 0.05 kg/m^3). Right panels show cross-section velocity sections (positive flow into the page). The relative position of the plan-view and section plots is indicated by white lines. Vertical section alignment is chosen to pass through both the anticyclone and the cyclone. Note that the domain centres move horizontally with the anticyclone centre.

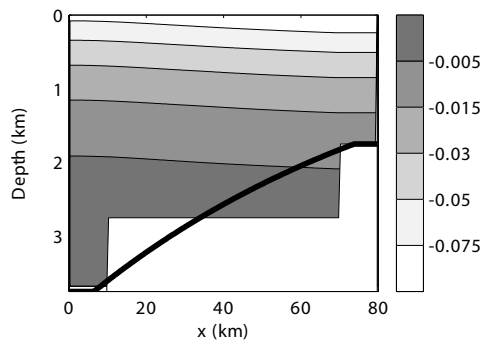


Figure 4: Section of initial density in the standard experiment. Density is relative to maximum (bottom) value. Bathymetry for “flat bottom” experiment is shown; bold line is bathymetry for standard sloping bottom experiment.

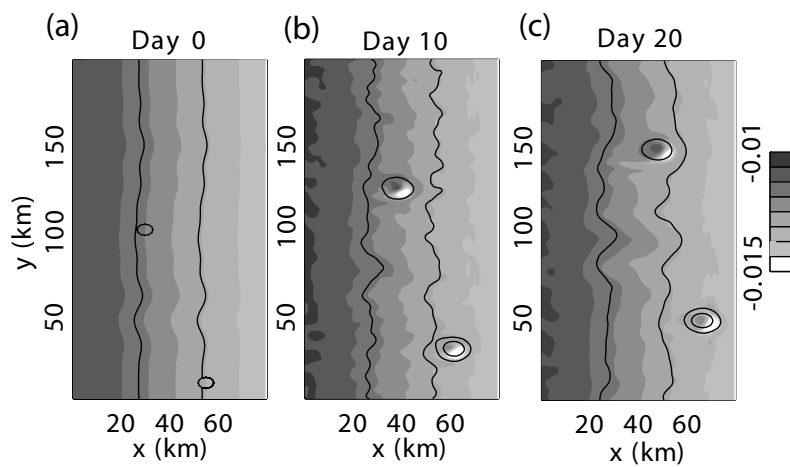


Figure 5: Density time slices from the early part of a mixed patch release experiment in the standard flat-bottom channel set-up. Density is at 1500 m, relative to the maximum density in the experiment. At this depth the anticyclones are lighter than the ambient water, and cyclones are denser than the ambient water. This level is below the maximum depth of the mixed patches before release (at $x = 30$ km, $y = 100$ km, and $x = 55$ km, $y = 10$ km). Black contours are for density at 400 m, and depict the upper ocean positive density anomaly associated with both cyclones and anticyclones.

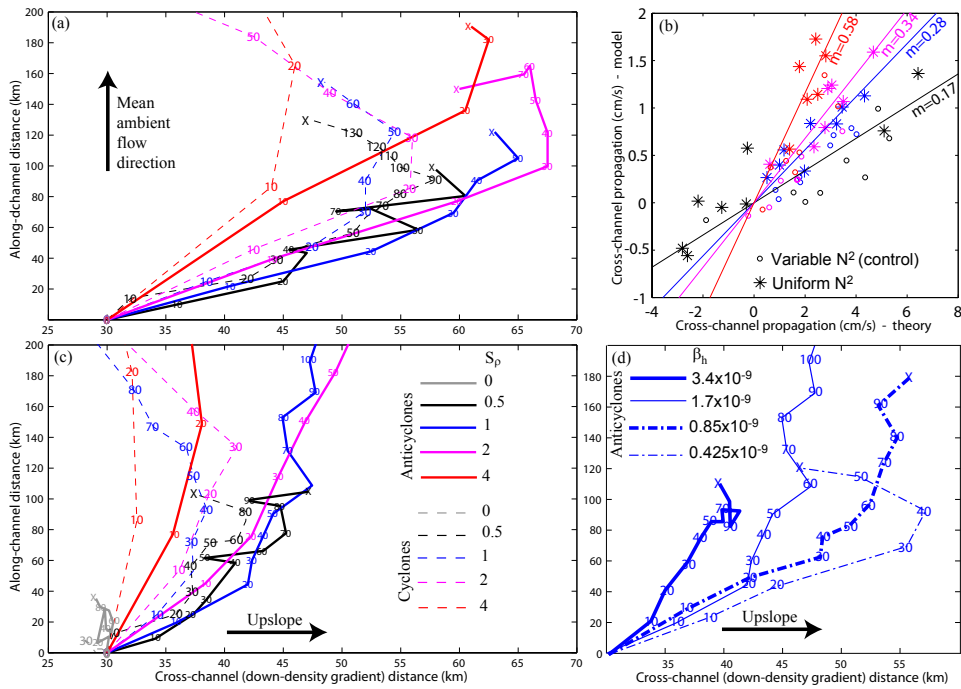


Figure 6: Trajectories of anticyclones and cyclones in (a) flat bottom experiments, and (c) sloping bottom experiments ($\beta_H = 1.7 \times 10^{-9}$). Trajectories are plotted for experiments where the horizontal stratification is scaled by $S_\rho = \frac{1}{2}, 1, 2$ and 4 respectively, relative to the standard experiment. Numbers indicate the day at which the vortex reached the specified location. An “X” indicates that the vortex has lost coherence. (b) - Model versus theoretical eastward propagation rates in flat bottom experiments. Colours indicate different values of S_ρ , matching those in (a) and (c). Circles are for variable N^2 experiments and stars for uniform N^2 experiments (see text). (d) - Trajectories of anticyclones in experiments over different values of slope steepness parameter β_H , with $S_\rho = 1$.

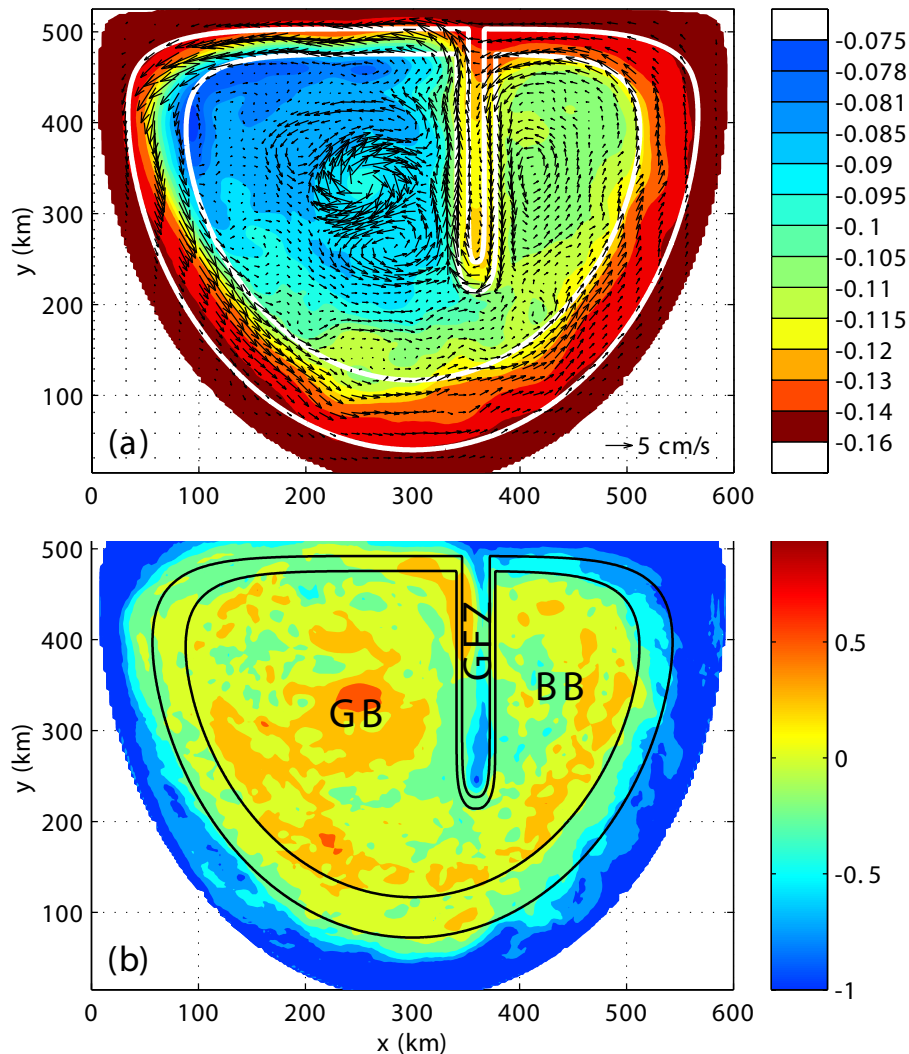


Figure 7: 200-400 day fields of (a) mean density, with velocity vectors (b) eddy kinetic energy ($\text{cm}^2 \text{s}^{-2}$; log scale) in the idealised bathymetry basin control experiment at 1250 m depth. Density is relative to the densest water in the basin. Velocity vectors are plotted at one twentieth of the resolution of the grid in both dimensions. 2000 m and 3000 m isobaths are plotted in white in (a); 2500 m and 3000 m isobaths are plotted in black in (b). The representation of the Greenland Basin (GB), the Boreas Basin (BB) and the GFZ are labelled in (b); the direction of north has been rotated so that the Greenland continental slope is at the upper limit of the plot.

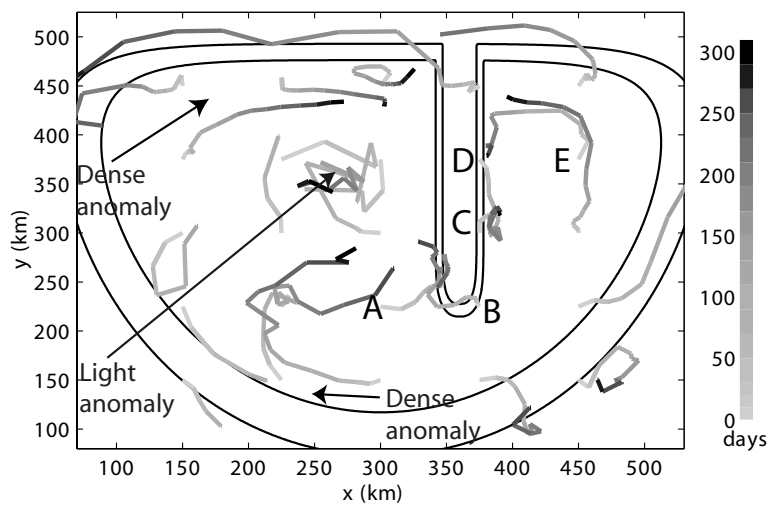


Figure 8: Spaghetti plot of anticyclone trajectories in the idealised bathymetry basin mixed-patch release experiment. Shading indicate number of days since the release of mixed patches. Some anticyclones lose coherence before the end of the experiment. 2500 m and 3000 m isobaths are plotted in black. Anticyclones that accumulate at the GFZ are labelled next to the start of their trajectories. Notable larger scale features are also labelled, where the horizontal density gradient is reversed relative to the general increase in density towards the geographical gyre centre (see Figure 7).

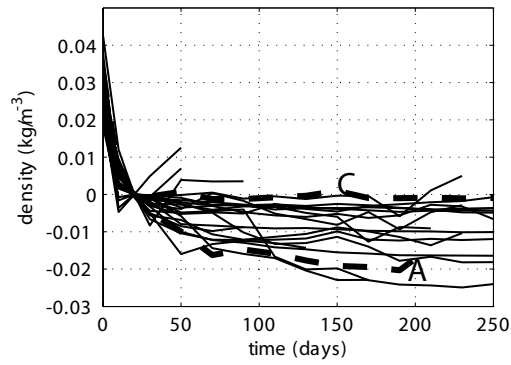


Figure 9: Evolution of density above each anticyclone at 400 m, referenced to density at Day 20 (after initial adjustment is complete), in the idealised bathymetry basin experiment. Incomplete tracks indicate that the anticyclone lost coherence. Anticyclones A and C (see Figure 8) are plotted with bold dashed lines.

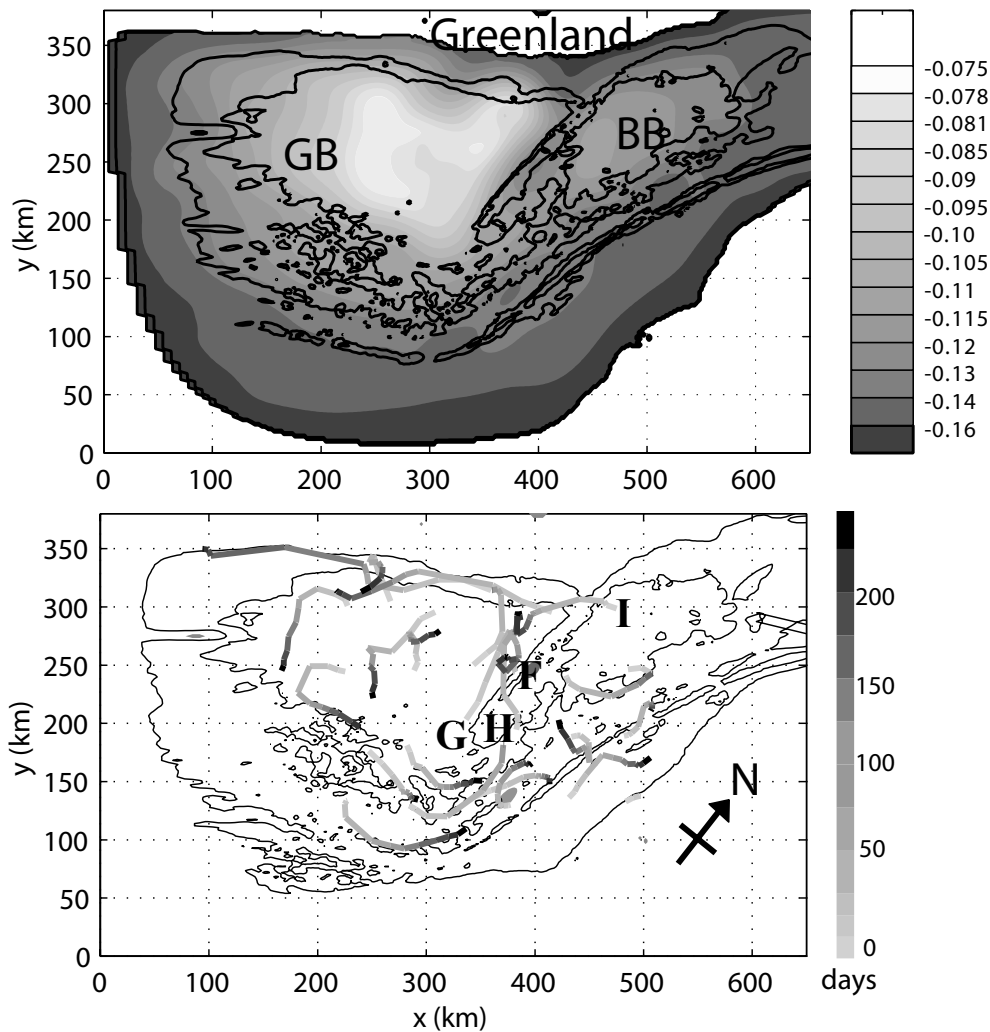


Figure 10: (a) 200-400 day mean density field in the realistic bathymetry basin control experiment at 1250 m depth. Density is relative to the densest water in the basin. 2500 m and 3000 m isobaths are plotted in black. (b) Spaghetti plot of anticyclone trajectories in the realistic bathymetry mixed-patch release basin experiment. Shading indicates the number of days since the release of mixed patches. Some anticyclones lose coherence before the end of the experiment. Anticyclones that become trapped at the GFZ are labelled in bold type next to the start of their trajectories.

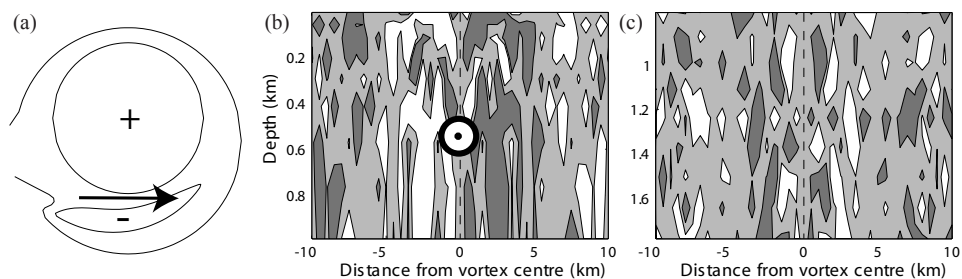


Figure 11: (a) - Plan view schematic of a quasi-monopole (after Voropayev et al., 1999). The arrow shows the direction of self-propagation. (b) - Vertical section of asymmetric relative vorticity, ζ , component (residual after symmetric component removed) through a composite of 26 surface cyclones that have recently separated from subsurface anticyclones upon interaction with topography. Section is viewed looking upslope. Dark shading indicates $\zeta > 0.3 \times 10^{-5}$; light shading indicates $0.3 \times 10^{-5} > \zeta > -0.3 \times 10^{-5}$. White shading indicates $\zeta < -0.3 \times 10^{-5}$. Implied dipole propagation, due to vortex asymmetry, is downslope (towards the reader). (c) - As (b) but a composite of 38 anticyclones.